

# Design and Analysis of Optical Planar Waveguide by Tapering Approach for Mid-infrared Supercontinuum Generation

M R Karim<sup>1</sup>, Nayem Al Kayed<sup>2</sup>,  
Md. Rabiul Hossain<sup>3</sup>, Golap Kanti Dey<sup>4</sup>

## Abstract

Varying dispersion and nonlinearity by tapering the thickness of a planar waveguide along the pulse propagation direction instead of keeping it uniform, create an opportunity to extend the supercontinuum spectral coverage further into the mid-infrared region. In this work, we numerically proposed a 5-mm-long group-velocity dispersion tailored silicon-rich nitride tapered waveguide for wideband supercontinuum coverage in the mid-infrared. Applying 50 fs FWHM sech pulses at the center of 1.55  $\mu\text{m}$  wavelength with a relatively low input power of 50 W, it was possible to achieve supercontinuum coverage from 0.8  $\mu\text{m}$  to 9  $\mu\text{m}$  by our proposed design. Besides, the results obtained using our proposed waveguide show that tapering the geometry enhances the supercontinuum coverage approximately 90% compared to a uniform waveguide of the same length. To the best of our knowledge, this would be the widest spectrum demonstrated ever using the tapered waveguide structure proposed so far. It may enable some spectacular mid-infrared region applications such as spectroscopic measurement, biomedical imaging, optical coherence tomography as well as sensing applications, etc.

## Keywords

Integrated photonic devices, nonlinear optics, silicon rich nitride, tapered planar waveguide, dispersion, nonlinearity, supercontinuum generation

## Introduction

Supercontinuum (SC) generation is obtained when a narrow but intense optical pulse propagates through a nonlinear medium. Interesting and visually realizable nonlinear effects play leading roles to generate SC inside the optical

<sup>1</sup> Associate Professor, School of Science & Engineering, Chittagong Independent University, Chattogram, Bangladesh.

<sup>2</sup> Department of Electrical and Electronic Engineering, Chittagong University of Engineering and Technology, Chattogram, Bangladesh

<sup>3</sup> Lecturer, School of Science & Engineering, Chittagong Independent University, Chattogram, Bangladesh.

<sup>4</sup> Assistant Professor, School of Science & Engineering, Chittagong Independent University, Chattogram, Bangladesh.

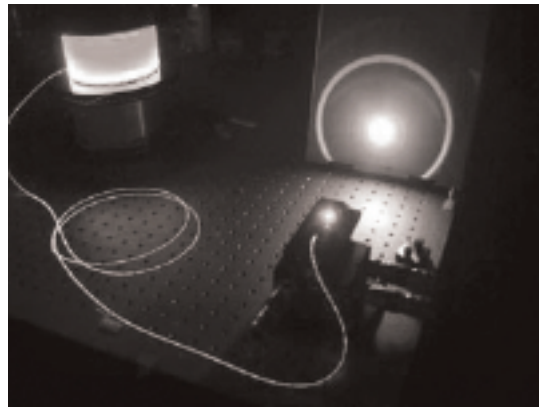
---

Corresponding author:

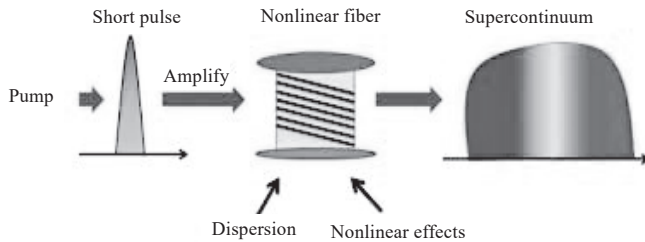
M R Karim, Associate Professor, School of Science & Engineering,  
Chittagong Independent University, Chattogram, Bangladesh.

Email: mrkarim@ciu.edu.bd

medium. In the early 1970s, the first-time broad continua were observed in the bulk medium by Alfano and Shapiro (1970) which was later recognized as the pioneering discovery in the nonlinear optics and gradually became the spectacular research field for the SC generation from ultraviolet (UV) to mid-infrared (MIR) region. The remarkable work of Ranka et al. (2000) producing an SC spectrum using photonic crystal fibers has driven the research field in a new direction. The technological development has enabled the researchers to look for the more desired and accessible optical spectrum using different types of optical materials and propagation mediums (Coen et al., 2001).



(a)



(b)

**Figure 1:** (a) An Experimental Setup of Continuous SC. Images Courtesy of Universit'e Lille; (b) An Illustration of SC Evolution.

Due to the advancement of technology in recent years, the degree of interest in ultrafast optics has increased to find out efficient broadband light sources (Dudley et al., 2006). The demand for versatile light sources increased because of the frequent usage of these sources in spectroscopy, telecommunication, biomedical imaging, and optical metrology applications (Petersen et al., 2018). Since all the molecules having strong vibrational absorption in the MIR region with the spectral range between  $2\ \mu\text{m}$  and  $20\ \mu\text{m}$ ; researchers find the center of interest nowadays to develop broadband SC light sources for the MIR spectroscopic applications (Dudley & Taylor, 2009).

The diverse range of application of the SC light sources has generated a feedback cycle whereby the scientists are requiring a better and efficient SC spectrum to match their specific requirement (Halir et al., 2012). The demand has motivated researchers to find new ways and create new novel methods to design the SC light sources as well as to develop theories for a deeper understanding of the formation of SC to aid in future advancement. In the last decades, the SC has not only been generated using the fiber mediums but it has also deployed the integrated waveguides which have opened the door for the generation of an efficient ultrabroadband SC spectrum by ensuring economical, compactness, robustness, stability and mass production ability consideration (DeVore et al., 2012). The experimental demonstration of SC evolution with graphical illustration (Liu et al., 2019) is depicted in Fig. 1.

To accomplish the optical planar waveguide-based SC generation in the MIR range, recent advancement on integrated photonics compatible technology has given a fantastic opportunity to fabricate versatile scale chip-based photonic devices. At present, complementary metal oxide semiconductor (CMOS) based platform can be made using Si (Leo et al., 2014), SiO<sub>2</sub> (Oh et al., 2014), high index doped SiO<sub>2</sub> (Duchesne et al., 2010), Si<sub>3</sub>N<sub>4</sub> (Ahmad et al., 2019; Wang et al., 2015; Liu et al., 2016), and chalcogenide (Xie et al., 2014; Karim et al., 2017). An intense investigation has made on a silicon-on-insulator (SOI) platform to create various scalable versatile silicon photonics devices considering their linear or nonlinear characteristics (Baehr-Jones et al., 2012). The ratio 2:1 between silicon and nitrogen creates a large bandgap of 2.05 eV which eliminates the two-photon absorption in silicon-rich nitride (SRN) compound at the 1.55 μm wavelength (Yang et al., 2018).

Besides, the SRN glass material has a large Kerr index of  $n_2 = 2.8 \times 10^{-13}$  cm<sup>2</sup>/W (four-times larger than Si) along with high material refractive index of 3.1 at the 1.55 μm wavelength, which is to be more suitable for dispersion optimization during photonic device design (Wang et al., 2015). The material absorption loss can be considered 6 dB/cm as Si-H bonds are introduced during fabrication (chemical vapor deposition) period (Ng et al., 2015).

To date, the SC evolution in the MIR employing SRN planar waveguides is reported in several research works (Wang et al., 2015; Liu et al., 2016). Wang et al. reported an SC spectral broadening from 1130 nm to 1750 nm using the SRN waveguide pumped at 1550 nm with a pulse of 500 fs duration at a peak power of 140 W (Wang et al., 2015). Liu et al. demonstrated an SC spectrum spanning from 820 nm to 2250 nm through 1 cm long SRN waveguide using an Er-Fiber laser pumped at 1555 nm with 105 fs duration pulses and an input peak power of 1330 W (Liu et al., 2016).

In this work, a 5-mm-long LiNbO<sub>3</sub> cladded SRN tapered planar waveguide is proposed for MIR SC generation. Applying thickness (H) tapering approach, we optimized a tapered waveguide by gradually varying its H. Using 50 W power with a full-width at half-maximum (FWHM) sech pulse of 50-fs width at the input of our proposed tapered waveguide, it is possible to obtain SC spanning from 0.8 μm to 9 μm which is 90% extra expansion compared to the

uniform waveguides of the same length. This can be the broadest expansion, to the best of the author's knowledge, by tapering a planar SRN waveguide in the MIR regime.

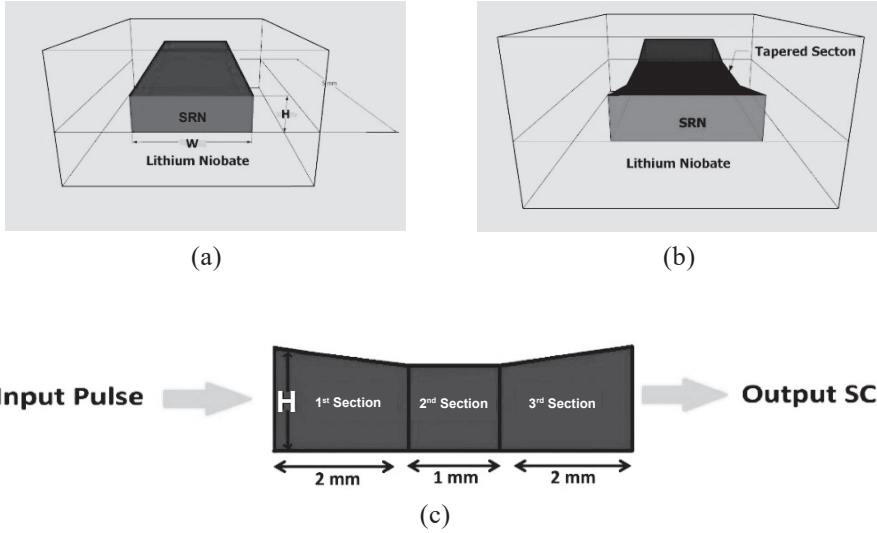


**Figure 2:** The Schematics of (a) A Uniform 3-D Waveguide; (b) Proposed 3-D Tapered Waveguide; (c) Longitudinal Cross-Section of the Waveguide Geometry along the Direction of Propagation Where  $H$  Varied for the: 1<sup>st</sup> Section between 600 nm and 500 nm (Down Tapering), 2<sup>nd</sup> Section Remains Constant at 500 nm, and 3<sup>rd</sup> Section Between 500 and 600 nm (Up Tapering).

## Modeling and Method

The schematics of our proposed structure are shown in Fig. 2. The waveguide core and claddings (both the upper and lower) are made of SRN and  $\text{LiNbO}_3$  respectively. Figures 2(a) and 2(b) are the 3D schematics of uniform and tapered geometries. Figure 2(c) depicts the longitudinal cross-section of the tapered structure. The core region of the geometry divided into three sections. Initial and final sections are down and up transition regions of each 2-mm-long and the middle part is a 1-mm-long uniform section, as illustrated in Fig. 2(c). For an initial section, down tapering is done by gradually varying  $H$  between 600 nm to 500 nm, and vice-versa is done for the final section (up tapering). The middle section remains uniform keeping  $H = 500$  nm along its length. Waveguide width,  $W$  is kept constant at 3000 nm throughout the analysis.

The linear refractive index estimations of the proposed materials are obtained by using the Sellmeier equations given in (Yang et al., 2018) and (Zelmon et al., 1997) for SRN and  $\text{LiNbO}_3$ , respectively. The Sellmeier coefficients of equations are mentioned in Table 1.

$$n(\lambda) = 1 + \sqrt{1 + \sum_{k=1}^N \frac{(a_k \lambda^2)}{\lambda^2 - \beta_k^2}} \quad (1)$$

$$n(\lambda) = \sqrt{1 + \sum_{k=1}^N \frac{(a_k \lambda^2)}{\lambda^2 - \beta_k^2}} \quad (2)$$

Where  $\lambda$  is the wavelength in  $\mu\text{m}$ .

**Table 1:** The Sellmeier Fitting Co-efficients

| Materials | SRN        |           | LiNbO <sub>3</sub> |           |
|-----------|------------|-----------|--------------------|-----------|
| N         | $\alpha_k$ | $\beta_k$ | $\alpha_k$         | $\beta_k$ |
| k=1       | 2.21715    | 0.0632602 | 2.67334            | 0.01764   |
| k=2       | 1.12108    | 0.249134  | 1.2290             | 0.054914  |
| k=3       | 24.8224    | 250.091   | 12.614             | 474.600   |
| k=4       | 17.6617    | 251.079   | –                  | –         |

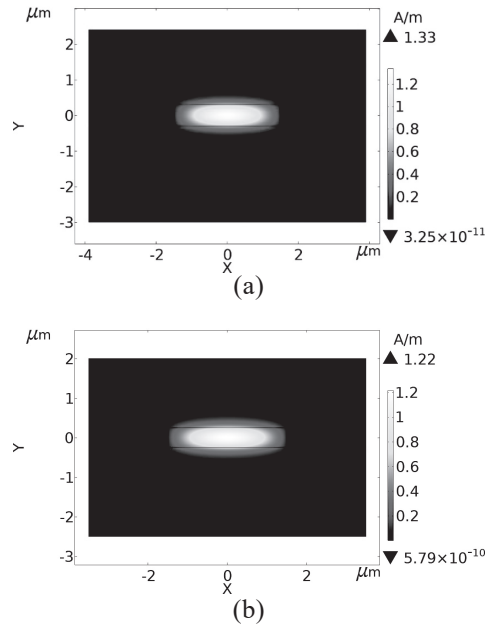


**Figure 3:** The FQTE Mode Profile of 1.55  $\mu\text{m}$  Wavelength for Structural Dimensions (a)  $W = 3 \mu\text{m}$  and  $H = 0.6 \mu\text{m}$ ; (b)  $W = 3 \mu\text{m}$  and  $H = 0.5 \mu\text{m}$ .

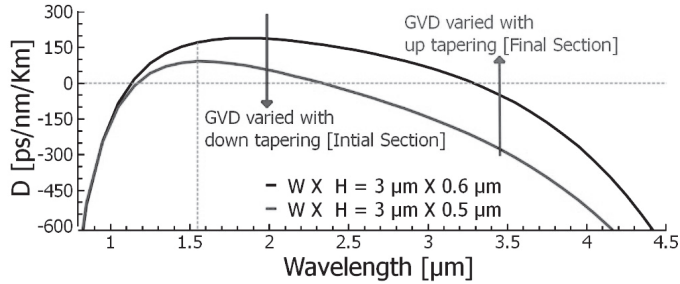
The effective refractive index of the tapered structure up to the desired wavelength region is calculated by using the finite-element method based COMSOL Multiphysics. The fundamental quasi transverse electric (FQTE,  $H_y^{\prime\prime}$ ) field mode profile patterns for the two different sections of our proposed waveguide at the wavelength of 1.55  $\mu\text{m}$  are depicted in Fig. 3. The FQTE mode profiles with the structural dimensions,  $W \times H = 3 \mu\text{m} \times 0.6 \mu\text{m}$  and  $W \times H = 3 \mu\text{m} \times 0.5 \mu\text{m}$  of the initial (starting point) and the ending (outgoing point) cross-sections of the down tapered region are shown in Figs. 3(a) and 3(b), respectively. The maximum magnetic field values at the 1.55  $\mu\text{m}$  wave length for the initial

and the ending cross-sections are 1.33 A/m and 1.22 A/m, respectively.

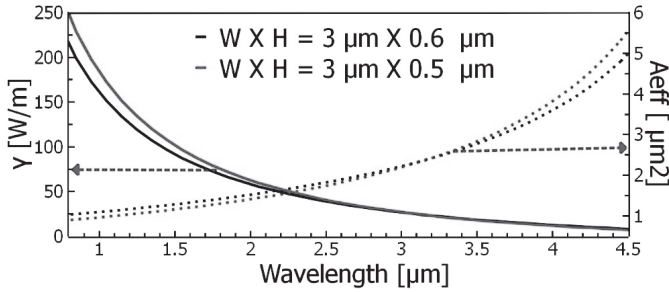
To study the evolution of the SC at the tapered waveguide output, a detailed investigation has been carried out by propagating a pulse in the waveguide anomalous dispersion region through numerically solving the generalized nonlinear Schrödinger equation (GNLSE) for one dimensional polarization (Gai et al., 2010). Due to the low Raman response of SRN material, the Raman terms in the GNLSE has been ignored (Ahmad et al., 2019).

$$\frac{\partial A}{\partial z} = -\frac{\alpha}{2} A + \sum_{k \geq 2}^{12} \frac{i^{k+1}}{k!} \beta_k \frac{\partial^k A}{\partial T^k} + i\gamma(|A|^2 A + \frac{i}{\omega_0} \frac{\partial}{\partial T} |A|^2 A) \quad (3)$$

In Eq. 3, the pulse envelop,  $A(z, T)$  evolves throughout the propagation direction along the proposed waveguide length in a retarded time frame,  $T = t - \beta_1 z$ , which moves at the group-velocity,  $v_g = \frac{1}{\beta_1}$ .  $\beta_k$  ( $k \geq 2$ ) is the higher-order GVD parameters estimated at the angular frequency,  $\omega_0$ . The linear material absorption loss of the SRN material is  $\alpha$ . The nonlinear co-efficient is given as,  $\gamma = \frac{n_2 \omega_0}{C A_{eff}}$ , where  $n_2$  is the Kerr-parameter at the angular frequency  $\omega_0$ . The mode effective area ( $A_{eff}$ ) for the waveguide fundamental mode up to the desired wavelength range is calculated by,  $A_{eff} = \frac{(\iint |E|^2 dx dy)^2}{(\iint |E|^4 dx dy)}$



(a)



(b)

**Figure 4:** (a) The GVD Curves for Two Different H as 500 nm (Grey Solid Line) and 600 nm (Black Solid Line) at  $W = 3000$  nm. The Vertical and Horizontal Dotted Lines Indicate the Pump Wavelength and the Zero-dispersion Level Respectively; (b) The Estimated Values of  $A_{eff}$  and  $\gamma$  are Plotted Corresponding to the GVD Curves Given in (a).

## Numerical Result

The most significant parameter for generating an effective SC with expansion up to the MIR region is GVD. The SC can be generated by optimizing the optical waveguide either in the all-normal GVD profile or in the anomalous GVD region. To achieve long-wavelength expansion up to the MIR, optimizing optical waveguide in the anomalous GVD is preferable than the normal dispersion region. During optimizing a waveguide in either of these GVD regions as well as to generate an effective SC at the waveguide output, it is very crucial to the placement of the pump source in the GVD profile. In this work, we optimized our proposed structure for pumping at the center wavelength of 1.55  $\mu\text{m}$  which is located in the anomalous GVD region. Another important aspect to generate effective SC spanning up to the MIR, the pump source has to be put near to the first zero-dispersion wavelength (ZDW), but in the longer wavelength side of the GVD curve. Initially, two uniform waveguide structures are optimized by taking H

For one structure as 600 nm and for other structure as 500 nm keeping W constant as 3000 nm for both the structures. Then, the tapering approach is followed to control both the dispersion and nonlinearity such that the SC coverage can be extended further in the MIR. The obtained GVD curves considering uniform approach with the waveguide structural dimensions,  $W \times H = 3 \mu\text{m} \times 0.6 \mu\text{m}$  and  $W \times H = 3 \mu\text{m} \times 0.5 \mu\text{m}$  are shown in Fig. 4(a). To control the GVD and the nonlinearity along the direction of propagation during the tapering waveguide design, H is gradually decreased from 600 nm to 500 nm up to 2 mm (1<sup>st</sup> section) of the total waveguide length. Following that H = 500 nm remains constant till 3 mm (2<sup>nd</sup> section) and then H starts to increase gradually up to 600 nm along the rest of the waveguide length (3<sup>rd</sup> section). The GVD for the tapered waveguide varies continually between the GVD curves (for initial section, GVD varies from black to grey curve and for final section, GVD varies from grey to black curve) shown in Fig. 4(a) throughout the tapered structure length. For the initial waveguide section, pump wavelength GVD value varies from 171 ps/nm/km to 91 ps/nm/km up to 2 mm of the waveguide and the next 1 mm continues with  $D = 91$  ps/nm/km for the 2<sup>nd</sup> section of the tapered waveguide. Pulse propagation in the final section continues with the varying GVD from 91 ps/nm/km to 171 ps/nm/km in the rest of the 2 mm waveguide. The corresponding mode effective area ( $A_{\text{eff}}$ ) and nonlinearity ( $\gamma$ ) plots for interesting wavelength region are depicted in Fig. 4(b). During the pulse propagation, the nonlinear coefficient at the pump wavelength varies from 87.2 /W/m to 96.6 /W/m in the first section and from 96.6 /W/m to 87.2 /W/m in the final section. The pulse in the middle section propagates with the constant nonlinear value of 96.6 /W/m.

To observe the SC spanning at the tapered waveguide output, the numerical analyses were carried out by solving the GNLSE Eq. 3 considering detailed assumptions described in Karim et al. (2017). The GNLSE was solved by adopting symmetrized split-step Fourier method (Karim et al., 2017). 217 number of grid points are considered to perform all simulations. The negative

frequency evolution was eliminated by considering 2.76 fs time step. The number of steps towards the pulse propagation direction are considered as  $10^5$  with a step-size of 100 nm. The terms associated with Raman effects are ignored during solving the GNLSE because of low Raman response of SRN material. The possible spurious SC outcome during computation are predicted and can be avoided by considering HOD up to 12<sup>th</sup> orders. The HOD values calculated and used during simulation are mentioned in Table 2.

**Table 2:** The HOD Values Considered During Simulations

| $\beta_k$<br>(psk/m) | W = 3 $\mu\text{m}$       |                           |
|----------------------|---------------------------|---------------------------|
|                      | H = 0.5 $\mu\text{m}$     | H = 0.6 $\mu\text{m}$     |
| $\beta_2$            | $-11.39 \times 10^{-2}$   | $-21.7 \times 10^{-2}$    |
| $\beta_3$            | $1.7946 \times 10^{-4}$   | $5.5503 \times 10^{-4}$   |
| $\beta_4$            | $9.8414 \times 10^{-7}$   | $-3.4285 \times 10^{-7}$  |
| $\beta_5$            | $-5.2454 \times 10^{-9}$  | $-8.0122 \times 10^{-11}$ |
| $\beta_6$            | $3.3958 \times 10^{-11}$  | $1.0954 \times 10^{-11}$  |
| $\beta_7$            | $-1.9870 \times 10^{-13}$ | $-9.3146 \times 10^{-14}$ |
| $\beta_8$            | $1.4391 \times 10^{-15}$  | $8.3490 \times 10^{-16}$  |
| $\beta_9$            | $-1.2784 \times 10^{-17}$ | $-8.9277 \times 10^{-18}$ |
| $\beta_{10}$         | $1.2744 \times 10^{-19}$  | $1.0184 \times 10^{-19}$  |
| $\beta_{11}$         | $1.7349 \times 10^{-21}$  | $-1.4790 \times 10^{-21}$ |
| $\beta_{12}$         | $3.3806 \times 10^{-23}$  | $2.7112 \times 10^{-23}$  |

**Source:** The author.

For all numerical simulations, a 50-fs TE polarized FWHM sech pulse is applied at the center of 1.55  $\mu\text{m}$  with a 50 W power given as input. Throughout the analysis, total length of the waveguide is considered as 5 mm. The material absorption loss is taken as 6 dB/cm [19] at the pump source wavelength. Initially, spectral coverage for two uniform waveguides are simulated, as illustrated in Figs. 5(a) and 5(b). For the structural dimensions, W = 3  $\mu\text{m}$ , H = 0.6  $\mu\text{m}$ , SC has been obtained between 0.8  $\mu\text{m}$  and 2.3  $\mu\text{m}$  (-40 dB equivalent), as shown in Fig. 5(a). For the next uniform structure, W = 3  $\mu\text{m}$ , H = 0.5  $\mu\text{m}$ , which is located at the end of down tapering region continued until 1 mm in the direction of propagation, the SC coverage can be achieved in the range 0.8-4.7  $\mu\text{m}$  (-40 dB equivalent), as shown in Fig. 5(b). From Figs. 5(a) and 5(b), we can say that if we consider any cross-section between the two uniform SRN waveguides considered above, we would not be able to achieve more SC extension than 4.7  $\mu\text{m}$ . However, by applying the tapering approach, the SC coverage can be extended further in the MIR region compared to a uniform waveguide of the same length, pulse width and peak power. In the case of the tapered waveguide for the same input peak power and pulse width, it has been possible to obtain the SC coverage from 0.8  $\mu\text{m}$  to 9  $\mu\text{m}$ , as shown in Fig. 5(c). It became possible

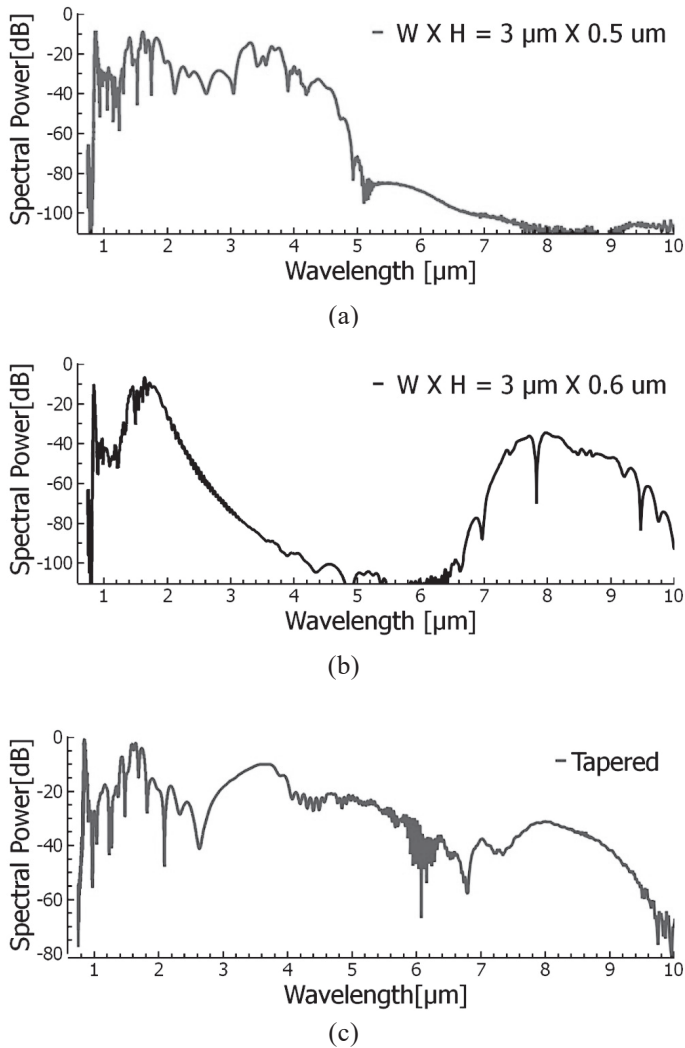


**Figure 5:** Spectral Coverage from a 5-mm-long Waveguide Output (a) with  $H = 600$  nm while Structure Remains Uniform; (b) with  $H = 500$  nm while Structure Remains Uniform; (c) while Tapering a Waveguide with the Variation of  $H$  between 600 nm and 500 nm.

to obtain such an extension through controlling GVD and nonlinear co-efficient throughout the whole length of the tapered waveguide. It is noticed that after tapering the waveguide, the SC coverage is increased further in the MIR region, which is approximately 90% more expansion compared to the uniform waveguide of the same length. Therefore, it is found tapering approach helps to achieve longer SC expansion compared to the uniform waveguide of same length and identical input peak power. Finally, the possibility of further coverage of SC bandwidth is investigated by increasing input peak power from 50 W

to 1000 W. Increment of input peak power to a moderate level shows that SC coverage can be obtained up to 16  $\mu\text{m}$  which will cross the transmission limit of the material we have proposed for our design.

## Conclusion

In this work, we theoretically generate MIR SC up to 9  $\mu\text{m}$  by using a 5-mm-long tapered waveguide made of SRN material as a core and  $\text{LiNbO}_3$  as top and bottom claddings. The proposed waveguide is tailored for pumping at the center of 1.55  $\mu\text{m}$  wavelength by applying the thickness tapering approach. Tapering of the waveguide provides the variation of dispersion and nonlinearity while the optical pulse propagates inside it resulting in a large SC expansion with same pulse duration and peak power compared to a uniform waveguide of same length. Thus, applying the tapering technique, it could be possible to obtain 90% more SC expansion in the MIR than uniform waveguide design. According to the authors' knowledge, this would be the widest SC expansion in the MIR by the tapered SRN waveguide with a relatively low peak power of 50 W. This numerical demonstration will pave the way to generate more SC expansion into the MIR using nonuniform SRN waveguide with the thickness tapering approach. The obtained SC may be a promising candidate for some spectacular MIR applications.

## References

- Ahmad, H., Karim, M. R., & Rahman, B. M. A. (2019). Dispersion-engineered silicon nitride waveguides for mid-infrared supercontinuum generation covering the wavelength range 0.8-6.5  $\mu\text{m}$ . *Laser Physics*, 29(2), 025301.
- Alfano, R. R., & Shapiro, S. L. (1970). Emission in the region 4000 to 7000  $\text{\AA}$  via four-photon coupling in glass. *Phys. Rev. Lett.*, 24, 584-587.
- Baehr-Jones, T., Pinguet, T., Guo-Qiang, P. L., Danziger, S., Prather, D., & Hochberg, M. (2012). Myths and rumours of silicon photonics. *Nature Photonics*, 6(4), 206.
- Coen, S., Chau, A. H. L., Leonhardt, R., Harvey, J. D., Knight, J. C., Wadsworth, W. J., & Russell, P. S. J. (2001). White-light supercontinuum generation with 60-ps pump pulses in a photonic crystal fiber. *Opt. Lett.*, 26(17), 1356-1358.
- DeVore, P. T. S., Solli, D. R., Ropers, C., Koonath, P., & Jalali, B. (2012). Stimulated supercontinuum generation extends broadening limits in silicon. *Applied Physics Letters*, 100(10), 101111.
- Duchesne, D., Peccianti, M., Lamont, M. R., Ferrera, M., Razzari, L., L'egar'e, F., Morandotti, R., Chu, S., Little, B. E., & Moss, D. J. (2010). Supercontinuum generation in a high index doped silica glass spiral waveguide. *Optics Express*, 18(2), 923-930.
- Dudley, J. M., Genty, G., & Coen, S. (2006). Supercontinuum generation in photonic crystal fiber. *Rev. Mod. Phys.*, 78, 1135-1184.
- Dudley, J. M., & Taylor, J. R. (2009). Ten years of nonlinear optics in photonic crystal fibre. *Nature Photonics*, 3(2), 85.

- Gai, X., Madden, S., Choi, D. Y., Bulla, D., & Luther-Davies, B. (2010). Dispersion engineered Ge<sub>11.5</sub>As<sub>24</sub>Se<sub>64.5</sub> nanowires with a nonlinear parameter of 136 /W/m at 1550 nm. *Optics Express*, 18(18), 18866-18874.
- Halir, R., Okawachi, Y., Levy, J. S., Foster, M. A., Lipson, M., & Gaeta, A. L. (2012). Ultrabroadband supercontinuum generation in a cmos compatible platform. *Opt. Lett.*, 37(10), 1685-1687.
- Karim, M. R., Ahmad, H., & Rahman, B. M. A. (2017). All-normal-dispersion chalcogenide waveguides for ultraflat supercontinuum generation in the mid-infrared region. *IEEE Journal of Quantum Electronics*, 53(2), 1-6.
- Leo, F., Safioui, J., Kuyken, B., Roelkens, G., & Gorza, S. P. (2014). Generation of coherent supercontinuum in a-si:h waveguides: Experiment and modeling based on measured dispersion profile. *Opt. Express*, 22(23), 28997-29007.
- Liu, X., Pu, M., Zhou, B., Krüchel, C. J., Fülöp, A., Bache M. et al. (2016). Octave-spanning supercontinuum generation in a silicon-rich nitride waveguide. *Optics Letters*, 41(12), 2719-2722.
- Liu, H., Yu, Y., Song, W., Jiang, Q., & Pang, F. (2019). Recent development of flat supercontinuum generation in specialty optical fibers. *Opto-Electronic Advances*, 2(2), 180020.
- Oh, D. Y., Sell, D., Lee, H., Yang, K. Y., Diddams, S. A., & Vahala, K. J. (2014). Supercontinuum generation in an on-chip silica waveguide. *Opt. Lett.*, 39(4), 1046-1048.
- Petersen, C. R., Prtljaga, N., Farries, M., Ward, J., Napier, B., Lloyd, G. R., Nallala, J., Stone, N., & Bang, O. (2018). Mid-infrared multispectral tissue imaging using a chalcogenide fiber supercontinuum source. *Opt. Lett.*, 43(5), 999-1002.
- Ranka, J. K., Windeler, R. S., & Stentz, A. J. (2000). Visible continuum generation in air-silica microstructure optical fibers with anomalous dispersion at 800 nm. *Optics Letters*, 25(1), 25-27.
- Xie, S., Tani, F., Travers, J. C., Uebel, P., Caillaud, C., Troles, J., Schmidt, M. A., & Russell, P. S. (2014). As<sub>2</sub>S<sub>3</sub>-silica double-nanospike waveguide for mid-infrared supercontinuum generation. *Opt. Lett.* 39(17), 5216-5219.
- Yang, M., Xu, L., Wang, J., Liu, H., Zhou, X., Li, G., & Zhang, L. (2018). An octave-spanning optical parametric amplifier based on a low-dispersion silicon-rich nitride waveguide. *IEEE Journal of Selected Topics in Quantum Electronics*, 24(6), 1-7.
- Zelmon, D. E., Small, D. L., & Jundt, D. (1997). Infrared corrected Sellmeier coefficients for congruently grown lithium niobate and 5 mol.% magnesium oxide-doped lithium niobate. *JOSA B*, 14(12), 3319-3322.